Journal of Water Process Engineering 81 (2026) 109293

Contents lists available at ScienceDirect

Journal of Water Process Engineering

journal homepage: www.elsevier.com/locate/jwpe

Tunable photoelectrocatalytic oxidation of chitosan/lignin coating on PVDF hollow fiber membrane for efficient oil-water separation

Sin Ling Chiam [a], Pei Yee Wong [a], Yan Xu [a], C.P. Leo [a,*], Swee-Yong Pung [b]

[a] School of Chemical Engineering, Engineering Campus, Universiti Sains Malaysia, 14300, Nibong Tebal, Pulau Pinang, Malaysia
[b] School of Materials and Mineral Resources Engineering, Engineering Campus, Universiti Sains Malaysia, Nibong Tebal, Pulau Pinang, Malaysia

ARTICLE INFO

Editor: Tzyy Haur Chong

Keywords:
PVDF membrane
Chitosan
Lignin
Photoelectrocatalysis
Oil removal

ABSTRACT

The oily wastewater presents serious environmental and operational challenges due to its stable emulsions and resistance to degradation. Commercial polymeric membranes, such as polyvinylidene fluoride (PVDF) membranes, could be used to remove oil through microfiltration. However, most of them are susceptible to severe fouling due to inherent hydrophobicity. In this study, a surface modification strategy was developed by coating PVDF hollow fiber membranes with a biopolymer blend of chitosan and lignin, followed by photoelectrocatalytic oxidation to tune surface properties. The biopolymer blend coating with oxidized functional groups showed changes in surface wettability. The photoelectrocatalytic oxidation using TiO_2/H_2O_2 slurry under UV irradiation and a 3 V bias generates surface hydroxyl radicals, further increasing wettability and enhancing membrane performance. Among the biopolymer coatings, a 1:1 chitosan–lignin ratio exhibited optimal performance. The modified membrane achieved a permeate flux of 1.6862 $L{\cdot}m^{-2}{\cdot}h^{-1}$, oil rejection of 99.26 %, and a reduced water contact angle of 17.34° after photoelectrocatalytic oxidation (4 h UV, 0.6 g/L TiO_2, 1.0 vol% H_2O_2). The photoelectrocatalytic oxidation of biopolymer-coated membranes offers tunable membrane surface properties. The synergy between biopolymer coating and photoelectrocatalytic oxidation offers a green, scalable route to fabricate biopolymer membranes with tunable properties for oily wastewater treatment.

1. Introduction

The oily wastewater from the edible oil industry is a continuous environmental challenge, requiring a great amount of chemicals and energy to remove the oil. In addition, the used cooking oil from households and restaurants not only enters sewage systems, but also natural water bodies. Oily wastewater contains high concentrations of oils, fats, and organic pollutants with high COD and BOD levels, which deteriorate aquatic ecosystems, promote bioaccumulation, and pose risks of contaminating drinking water sources [1]. The persistent emulsions and poor biodegradability of oily wastewater require effective treatment strategies. Various techniques such as flotation, coagulation, biological treatments, and adsorption have been employed for oily wastewater remediation [2,3]. However, many of these methos suffer from drawbacks, including limited separation efficiency, high chemical demand, and secondary pollution. Membrane filtration has emerged as a robust and energy-efficient solution in recent years. Membranes can selectively separate oil droplets and suspended solids from water, making them ideal for treating oil-laden effluents [4–6].

Commercial membranes are mostly produced from synthetic polymers, including polyvinylidene fluoride (PVDF), polysulfone (PSf) [7], polyethersulfone (PES) [8], and polypropylene (PP) [9], due to their excellent chemical resistance, thermal stability, and mechanical strength under harsh operating conditions [10,11]. Despite these advantages, these membranes are inherently hydrophobic, which promotes oil fouling and reduces water permeability. This leads to increased cleaning costs and a shortened membrane lifespan. To overcome these limitations, different strategies of membrane modification have been widely explored to improve membrane hydrophilicity and fouling resistance without altering bulk membrane integrity for filtering oily wastewater. In this context, natural biopolymers at a low cost have been explored. Chitosan, derived from crustacean shells, is rich in amino ($–NH_2$) and hydroxyl (–OH) groups that improve water affinity [12]. Liu et al. [13] precipitated an alkaline chitosan dope solution in an ethanol coagulation bath at low temperature to form a chitosan membrane. The chitosan membrane with hierarchical morphology could reject bovine serum albumin effectively. Hardian et al. later [14] fabricated a chitosan/cellulose membrane with an oil removal efficiency of 44 % through

* Corresponding author.
E-mail address: chcpleo@usm.my (C.P. Leo).

https://doi.org/10.1016/j.jwpe.2025.109293
Received 18 September 2025; Received in revised form 5 December 2025; Accepted 8 December 2025
Available online 17 December 2025

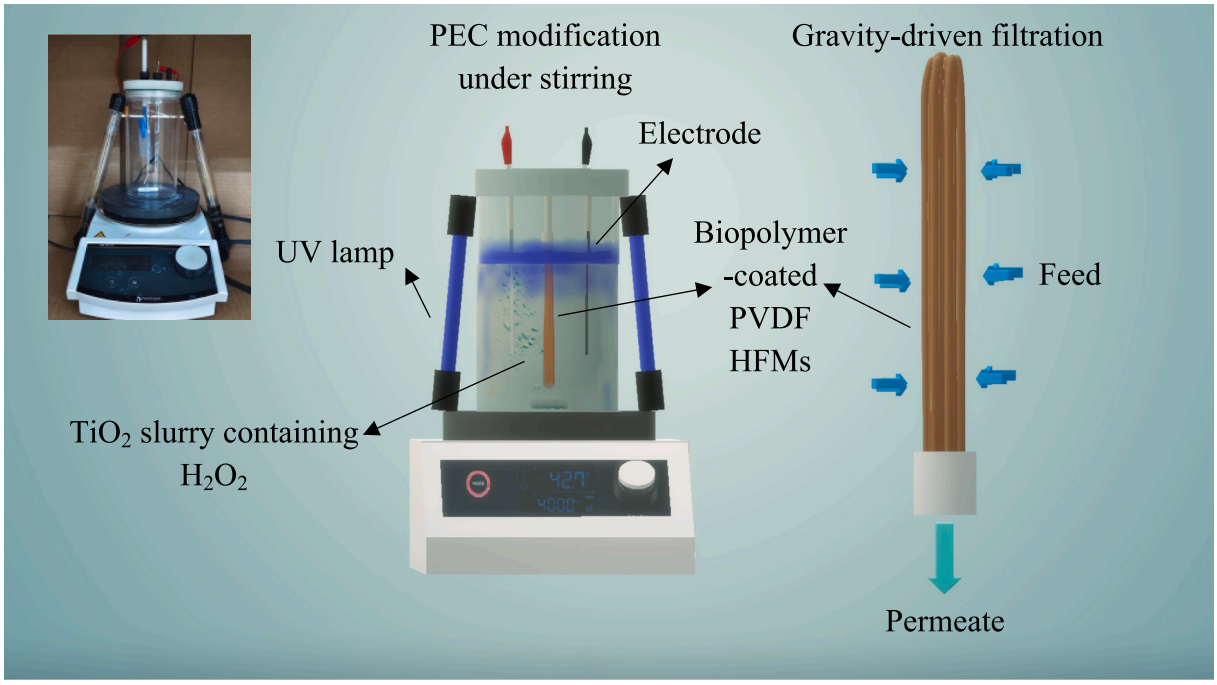

Fig. 1. Schematic illustration of the PEC modification and gravity-driven filtration using lignin and/or chitosan-modified PVDF HFMs.

phase inversion as well. Chitosan and cellulose were dissolved in dimethyl sulfoxide containing [Bmim][OAc] ionic liquid, before casting on PP support and precipitating in water. During phase inversion, chitosan derivatives such as carboxymethyl chitosan or chitosan quaternary ammonium salt were added into the aqueous bath to manipulate the phase inversion of the PES dope solution to form an oil separation membrane [15]. Polyvinylpyrrolidone (PVP) was added to the dope solution as the chitosan derivatives could crosslink PVP through the formation of hydrogen bonding to construct a hydrophilic coating on the PES membrane. In addition, chitosan hydrogel was coated onto alkali-treated PVDF membrane, which was enriched with –OH, Cu^{2+}, which could form coordination bonds with –OH, chitosan, and dopamine [16]. Due to the formation of an underwater superoleophobic surface, the chitosan hydrogel-coated membrane attained a flux recovery ratio (*FRR*) of 90.3 % even after 10 cycles of filtration. A chitosan membrane could also be fabricated through electrospinning. Zeng et al. [17] added poly (ethylene oxide) into the acetic acid to form the spinnable chitosan solution, besides CNC, which could increase membrane hydrophilicity. The chlorinated chitosan membrane removed more than 85 % of oil in the aqueous feed. Chlorination reduced the hydrogen bond and electrostatic interaction involving $–NH_2$ within chitosan to prevent premature fiber cracks caused by the excessive hydrogen bond.

Recent studies have also explored light-driven modification of biopolymeric coatings to further enhance membrane functionality. Xu et al. [18] valorized, cleaned, and regenerated lignin-coated PVDF membranes in the TiO_2 slurry through photocatalytic and photoelectrochemical approaches. The lignin coating could be valorized through cleavage of C—O and C—C bondings, while cleaning was mainly driven by reactive oxygen species (ROS) such as hydroxyl (•OH) and superoxide radicals ($•O_2^-$) during photocatalytic or photoelectrocatalytic treatment. The lignin coating could even be degraded to regenerate PVDF membranes for reuse purposes after recoating. Similar to lignin, chitosan could be readily valorized by oxidation since past studies have shown the effectiveness of H_2O_2 in the manipulation of molecular weight [19]. The treated chitosan samples showed new carboxyls and reduced amines. Chitosan is a cationic biopolymer with abundant amino ($–NH_2$) and hydroxyl (–OH) groups, which can undergo oxidation. The additional UV irradiation promoted the generation of hydroxyl radicals from H_2O_2 to attack the β-D-(1 → t) glucosidic bondings in chitosan [20]. The oxidation of chitosan using H_2O_2 could be even promoted by peroxomolybdate catalysts [21]. Since different biopolymers with varied functional groups have different oxidation mechanisms and rates, the membranes coated with biopolymer blends should be further explored. It is important to understand the effects of different functional groups generated through oxidation on membrane filtration and fouling behaviors. In addition, the cleaning and degradation mechanisms are helpful in designing durable biopolymer membranes. Templating effects can even be attained after degrading one of the biopolymers.

Hence, this study focuses on the oxidation of lignin/chitosan blend-coated PVDF membrane. The present study also includes the photoelectrocatalytic (PEC) activation during the oxidation of lignin/chitosan coatings. Unlike conventional PEC systems that operate during filtration for pollutant and cleaning purposes [22–24], this study applies PEC to modify biopolymer membranes for chemical modification of the membrane surface. By combining UV irradiation, TiO_2 photocatalysis, hydrogen peroxide, and applied voltage, the PEC system generates reactive oxygen species (•OH, O_2^-) that oxidatively tune surface energy and wettability. This pre-treatment strategy facilitates precise control over the lignin-chitosan modified PVDF hollow fiber membrane (LigCS-PVDF HFMs) surface for oil–water separation. By bridging the aforementioned gaps, the present work offers a surface modification paradigm that is scalable, green, and adaptable. The resulting membranes are evaluated in terms of hydrophilicity, oil–water separation performance, and long-term reusability, with emphasis on optimization of PEC operational parameters to ensure practical relevance. These findings are expected to provide new insights into the design of biopolymer-integrated membranes for sustainable oily wastewater treatment.

2. Materials and methods

2.1. Materials

PVDF hollow fiber membranes (HFMs) with a pore diameter of 0.1 μm, inner diameter of 1.5 mm, and outer diameter of 2.6 mm were acquired from Tuoyan Technology Co. Ltd. (China). Ethanol (C_2H_5OH,

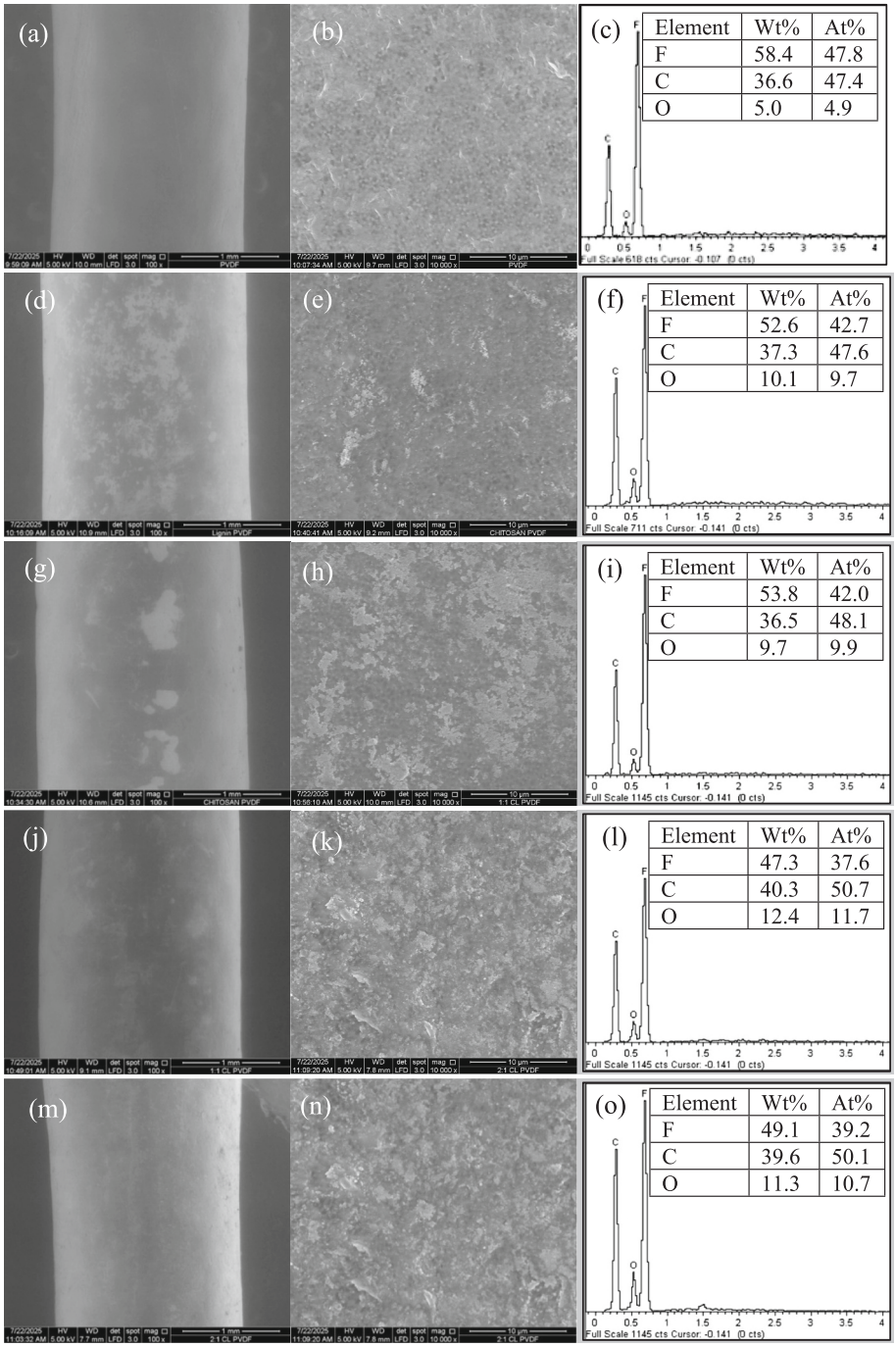

Fig. 2. SEM images and EDS analysis results of (a, b, c) pristine PVDF, (d, e, f) Lig-PVDF, (g, h, i) CS-PVDF, (i, j, k) Lig_1CS_1-PVDF, and (k, l, m) Lig_2CS_1-PVDF HFMs after PEC activation (4 h UV irradiation, 0.6 g/L TiO_2, 1.0 vol% H_2O_2, 3 V).

99.7 % purity, denatured) was purchased from R&M Chemicals (Malaysia). Lignin (purity ≥99.5 %) and food-grade chitosan were obtained from Guangdong Yunxing Biotechnology Co., Ltd. and Xi'an Lanshan Biotechnology Co., Ltd. (China), respectively. Acetic acid (CH_3COOH, purity ≥99 %) and sodium hydroxide (NaOH, analytical grade) were supplied by Sigma-Aldrich (USA) and R&M Chemicals (Malaysia), respectively. Titanium dioxide (TiO_2) nanoparticles with a particle size of 21 nm and purity ≥99.5 % (trace metal basis) were obtained from Sigma-Aldrich (USA). Hydrogen peroxide (H_2O_2, analytical grade) was sourced from QRëC (New Zealand), while sodium sulfate (Na_2SO_4, purity ≥99 %) was purchased from Sigma-Aldrich (USA). Corn cooking oil (100 %) and Tween 80 (analytical grade) used in oily wastewater preparation were obtained from ACH Food Companies, Inc. (USA) and Merck (Germany), respectively.

2.2. Coating of PVDF HFMs

PVDF HFMs were modified to enhance hydrophilicity and separation performance by applying biopolymer-based coatings comprising lignin and chitosan at different weight ratios. Membranes were first cut into uniform lengths of 70 cm. Before coating, membranes were cleaned by soaking in ethanol for 15 min to remove surface oils and contaminants, followed by rinsing with deionized water. The membranes were then air-dried at room temperature and stored in a clean, dust-free environment to ensure optimal adhesion during coating.

In the preparation of the pure lignin coating (Lig-PVDF HFMs), 7.5 g

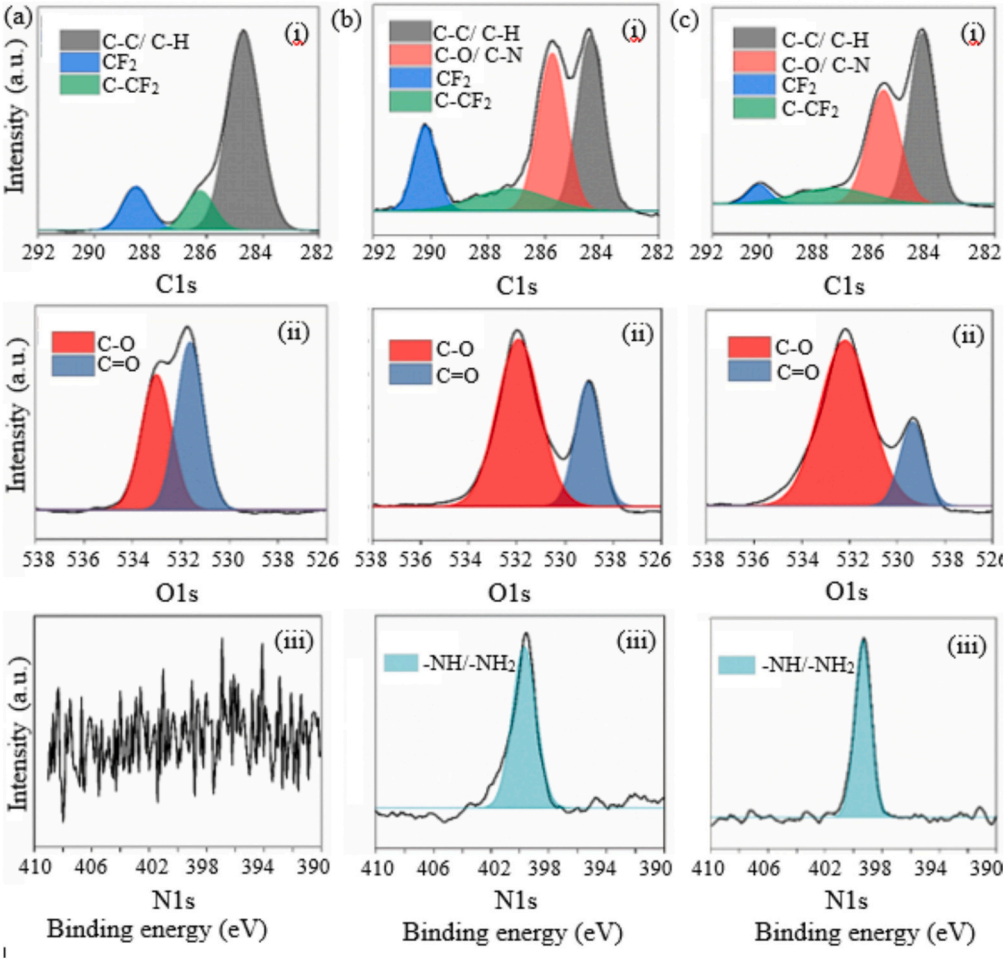

Fig. 3. High-resolution XPS spectra of (a) pristine PVDF, (b) Lig_1CS_1-PVDF, and PEC-modified Lig_1CS_1-PVDF HFMs (0.6 g·L^{-1} TiO_2, 1.0 vol% H_2O_2, 3 V, 4 h UV) with (i) C 1s, (ii) O 1s, and (iii) N 1s regions.

of lignin was dissolved in 1000 mL of distilled water containing 5 g of NaOH. The solution was continuously stirred until complete homogenization, yielding a stable dark-brown liquid. The pure chitosan coating (CS-PVDF HFMs) was prepared from 7.5 g of chitosan, which was added to a mixture of 10 mL of acetic acid and 1000 mL of distilled water. There were two types of lignin–chitosan blend coatings. For preparing lignin-chitosan blend coating at the ratio of 1:1 (Lig_1CS_1-PVDF HFMs), 3.5 g of lignin and 2.5 g of NaOH were dissolved in 500 mL of distilled water, while 3.75 g of chitosan was dissolved in 500 mL of distilled water containing 5 mL of acetic acid. The lignin-chitosan blend coating at the ratio of 2:1 (Lig_2CS_1-PVDF HFMs) was prepared similarly. 7.5 g of lignin and 5 g of NaOH were dissolved in 500 mL of water, while 3.75 g of chitosan was prepared in the same manner. For both blend coatings, the lignin and chitosan solutions were stirred individually until fully dissolved before mixing for at least 4 h to ensure uniform dispersion and compatibility of the two biopolymers.

PVDF HFMs were then immersed in the coating solution under stirring at room temperature for 24 h to ensure uniform adsorption of the coating materials. Following immersion, the membranes were rinsed with deionized water to remove loosely bound polymers and dried under ambient conditions for 24 h in a clean environment. The coated PVDF HFMs were then stored in sealed plastic containers until further photoelectrocatalytic treatment and filtration performance evaluations.

2.3. PEC treatment of lignin and/or chitosan-coated PVDF HFMs

PEC treatment was conducted through a series of parametric tests using lignin and/or chitosan-coated PVDF HFMs to understand the key parameters known to influence separation performance and fouling resistance in oil–water separation. The coated membranes were vertically immersed in 250 mL of an aqueous solution containing 0.2 to 1.0 g/L TiO_2, 1 M sodium sulfate (Na_2SO_4) as supporting electrolyte, and 0.5 to 2.0 vol% hydrogen peroxide (H_2O_2). Two UV lamps were positioned beside the membranes to ensure uniform irradiation across the membrane surface. A photoanode and a stainless steel metal cathode with dimensions of 2 cm × 4 cm were immersed in the solution and connected to a DC power supply to facilitate electrochemical reactions alongside photocatalysis. The solution was stirred throughout the treatment to maintain solution homogeneity while minimizing hydrodynamic disturbance at the membrane interface. The following sub-sections describe the individual experiments used to evaluate the effects of each parameter.

To study the effects of treatment duration, two pieces of coated PVDF HFMs were immersed in 250 mL of a solution containing 0.2 g/L of TiO_2 and 0.5 vol% of H_2O_2. A fixed voltage of 3 V was applied throughout. The membranes were exposed to UV light placed beside the beaker, with the treatment duration varied between 1 and 6 h. To understand the effects of TiO_2 loading on the PEC treatment, the concentration of TiO_2 was varied from 0.2 to 1.0 g/L while keeping the H_2O_2 concentration constant at 0.5 vol% and the applied voltage at 3 V under UV irradiation for 4 h. The effects of H_2O_2 were studied by varying the H_2O_2 volume fraction from 0.5 to 2.0 vol% while maintaining TiO_2 concentration at 0.6 g/L and a fixed applied voltage of 3 V under UV irradiation for 4 h. Lastly, the applied voltage was manipulated between 1 V and 5 V

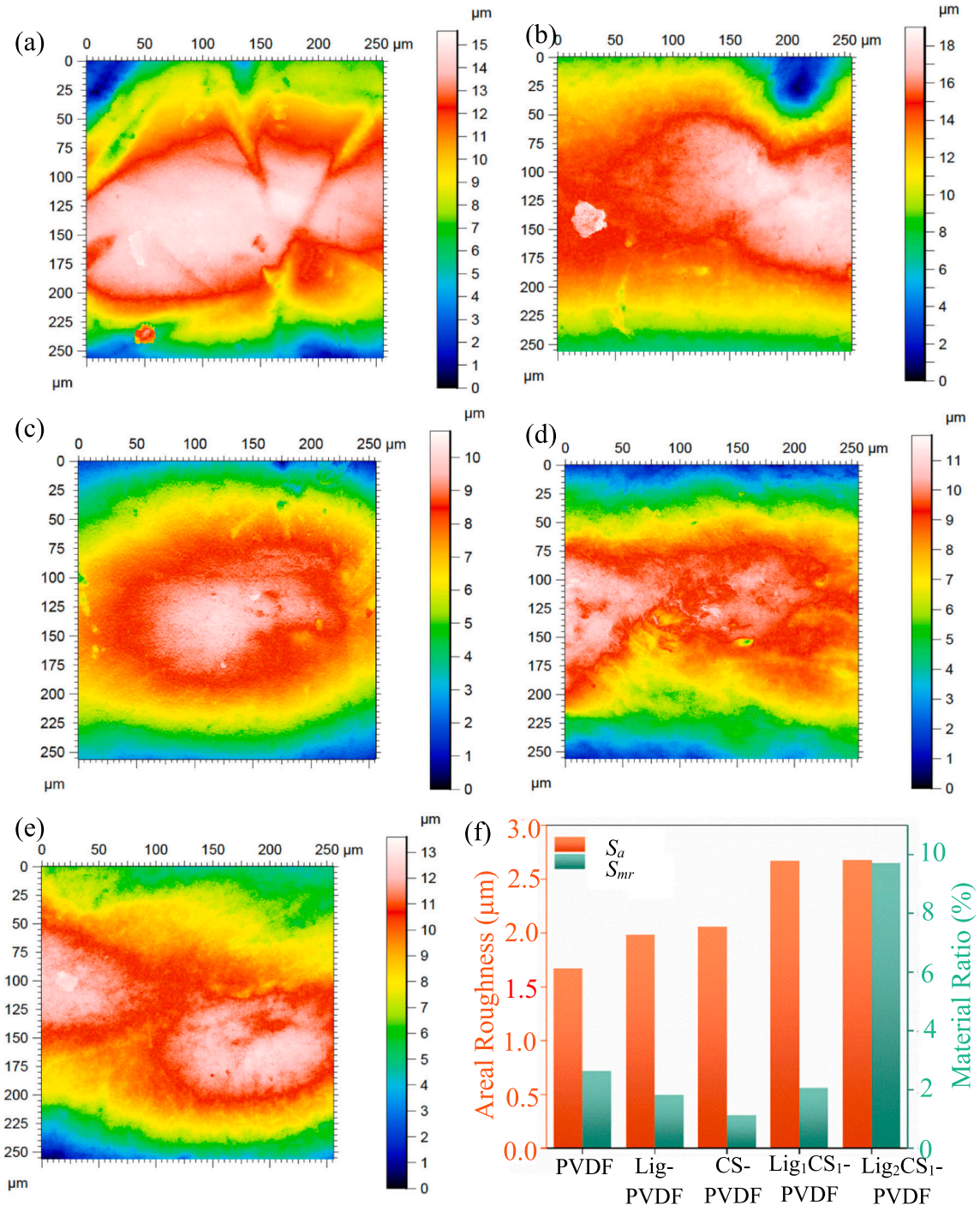

Fig. 4. LSM areal surface roughness analysis of (a) PVDF, (b) Lig-PVDF, (c) CS-PVDF, (d) Lig_1CS_1-PVDF, and (e) Lig_2CS_1-PVDF HFMs after PEC activation (0.6 g·L^{-1} TiO_2, 1.0 vol% H_2O_2, 3 V, 4 h UV). The height maps illustrate the surface topography over a 250 × 250 μm^2 area under identical scale and *Z*-range settings. (f) Areal roughness (S_a) and material ratio (S_{mr}) under ISO 25178 analysis.

applied across the electrodes to understand the effects of applied voltage on the PEC treatment. The TiO_2 and H_2O_2 concentrations were maintained at 0.6 g/L and 0.5 vol% under UV irradiation for 4 h, respectively.

To verify the involvement of reactive oxygen species (ROS) during the PEC activation process, scavenger inhibition tests were conducted. Three types of scavengers in 1 mL of test solution were introduced individually into the PEC treatment solution, namely tert-butanol (t-BuOH, 10 mM) as the hydroxyl radical (•OH) scavenger, p-benzoquinone (BQ, 1 mM) as the superoxide radical ($O_2^{\bullet -}$) scavenger, and ethylenediaminetetraacetic acid (EDTA, 1 mM) as the hole (h^+) scavenger. Lig1CS1-PVDF HFMs under the optimum treatment conditions were used in scavenger inhibition tests.

2.4. Characterization

The surface morphologies of samples were analyzed by field emission scanning electron microscopy (FESEM, Zeiss Supra 35 VP). The surface chemical composition and elemental states of the membranes were analyzed using a high-resolution multi-technique X-ray photoelectron spectrometer (XPS, Axis Ultra DLD, Kratos Analytical Ltd., UK)

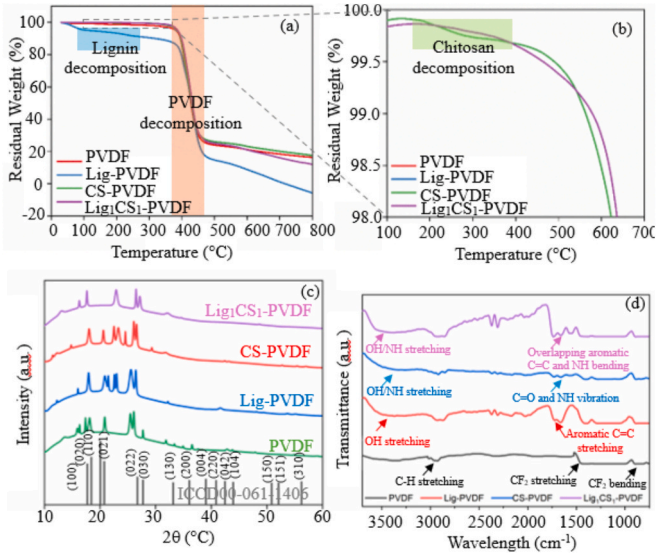

Fig. 5. TGA spectra with (a) full degradation range (30–800 °C) and (b) initial region highlighting weight losses from chitosan decomposition and moisture evaporation, (c) XRD, and (d) FTIR spectra of pristine and modified PVDF HFMs after PEC activation (0.6 g·L^{-1} TiO_2, 1.0 vol% H_2O_2, 3 V, 4 h UV).

equipped with a monochromatic Al Kα radiation source (1486.6 eV). The crystal structures were studied using an automated X-ray diffractometer (XRD) system (D8 Advance Bruker, Karlsruhe, Germany) with Cu-K_α radiation (15.4056 nm) at 40 kV and 40 mA, ranging from 20° to 90° at room temperature. Thermogravimetric analysis (TGA) was carried out using the SETSYS Evolution TGA system under a nitrogen atmosphere from room temperature to 900 °C at a heating rate of 20 °C/min. The covalent bonding interaction and functional group of samples were determined using a Fourier-transform infrared (FTIR) spectrometer (Nicolet IS10, USA). The surface roughness and topography of the membranes were examined using a confocal laser scanning microscope (CLSM, Zeiss LSM 700 MAT with Axio Imager. Z2 Vario, Germany). Three-dimensional surface profiles were captured over a 250 × 250 μm^2 area, and the data were analyzed using ConfoMap software (ISO 25178) to obtain the areal roughness (S_a) and material ratio (S_{mr}) parameters. The droplet size distribution of the oil-in-water emulsion before and after separation was determined using a laser diffraction particle size analyzer (CILAS 1180, France) based on the Fraunhofer optical model. The emulsion was further examined using a digital optical microscope (HiView Plus-WiFi).

Unless otherwise stated, all the lignin and/or chitosan-coated PVDF HFMs presented herein were characterized after PEC activation (4 h UV irradiation, 0.6 g/L TiO_2, 1.0 vol% H_2O_2, 3 V) to represent the final form of membranes in separation performance evaluation. The pristine PVDF HFM was characterized as the unmodified control HFM.

2.5. Performance tests

The performance of the coated PVDF HFMs was evaluated based on permeate flux, oil rejection, and water contact angle (WCA) measurements to assess filtration efficiency and surface wettability. All tests were conducted under controlled laboratory conditions using a standardized oil-in-water emulsion as the feed solution.

The permeate flux was measured during gravity-driven filtration using a dead-end setup, as shown in Video 1 (Supplementary data). The coated membrane was inserted into a 25 cm-long PTFE tube and sealed at one end with epoxy resin to prevent leakage. The feed solution was prepared by mixing 10 mL of deionized water, 1 mL of cooking oil, and 1.5 mL of Tween 80, stirred for 15 min to ensure homogeneous dispersion. During the test, the emulsion was introduced into the PTFE tube, and the permeate was collected at 2-h intervals. The permeate volume was recorded, and the permeate flux (J, L·m^{-2}·h^{-1}) was calculated using the following equation:

$$J = \frac{V}{A} \times t \quad (1)$$

where V is the permeate volume (L), A is the effective membrane area (m^2), and t is the filtration time (h).

The oil rejection efficiency was assessed by comparing the oil concentrations in the feed and permeate solutions. The oil-in-water emulsion was prepared as described above, with extended stirring for 30 min to ensure consistent dispersion. Following filtration, the permeate samples were analyzed using a UV–Vis spectrophotometer. Absorbance was measured at 225 nm, the characteristic wavelength for oil in aqueous systems. Prior to analysis, a calibration curve was established using standard oil-in-water solutions with known concentrations. The linear regression equation from the calibration, $y = 0.1081x + 0.03$ ($R^2 = 0.9969$), was used to determine the oil concentration in both feed (C_f) and permeate (C_p) samples. The oil rejection (R) was calculated using the equation:

$$R = \left(1 - \frac{C_p}{C_f}\right) \times 100\% \quad (2)$$

The membrane surface wettability was evaluated based on the WCA value. A droplet of 5 μL of deionized water was carefully deposited onto the membrane surface using a precision micro-syringe. The droplet was placed gently to avoid disturbance, and a side-view image was immediately captured using a high-resolution camera via the HiView mobile application. The WCA at the water–membrane interface was determined using the ImageJ software. The underwater oil contact angle (UWOCA) was measured using a goniometer (LSA 200, Lauda Scientific). The membranes were immersed in deionized water for 30 min and placed in a beaker filled with water. A droplet of oil (2 μL) was injected beneath the water phase, and the static contact angle was recorded within 5 s.

2.6. Stability tests

The reusability of the selected HFMs was assessed through multiple oil–water separation cycles. After each cycle, the membrane was rinsed thoroughly with deionized water, followed by measurements of oil rejection efficiency, permeate flux, and WCA to monitor performance stability over repeated use. The chemical stability was tested by immersing membranes in 1 M HCl, 1 M NaOH, and ethanol for 24 h. They were rinsed before the separation test and wettability measurement. Thermal stability was assessed by performing oil–water separation at 25, 40, 55, and 70 °C. The matrix stability tests were conducted using 5 wt% NaCl, 0.1 wt% SDS, as well as a mixture containing 5 wt% NaCl and 0.1 wt% SDS to simulate saline and surfactant-rich conditions. Each sample was pre-soaked for 1 h before testing to ensure equilibrium was reached.

3. Result and discussion

3.1. Characteristics of biopolymer-coated PVDF HMFs

Fig. 1 illustrates the overall synthesis and activation process used to fabricate the modified PVDF HFMs. Initially, the PVDF HFMs were coated with a biopolymer blend consisting of chitosan and lignin. Chitosan was dissolved in acetic acid to promote protonation of the amino groups [25], while lignin was dispersed in alkaline media to facilitate solubility [26]. Upon mixing, the blend was applied onto the PVDF surface, forming a functionalized coating layer through hydrogen bonding, π–π stacking, van der Waals forces, and electrostatic interactions with the membrane substrate [27]. The coated membranes were then subjected to PEC activation by immersion in a TiO_2/H_2O_2

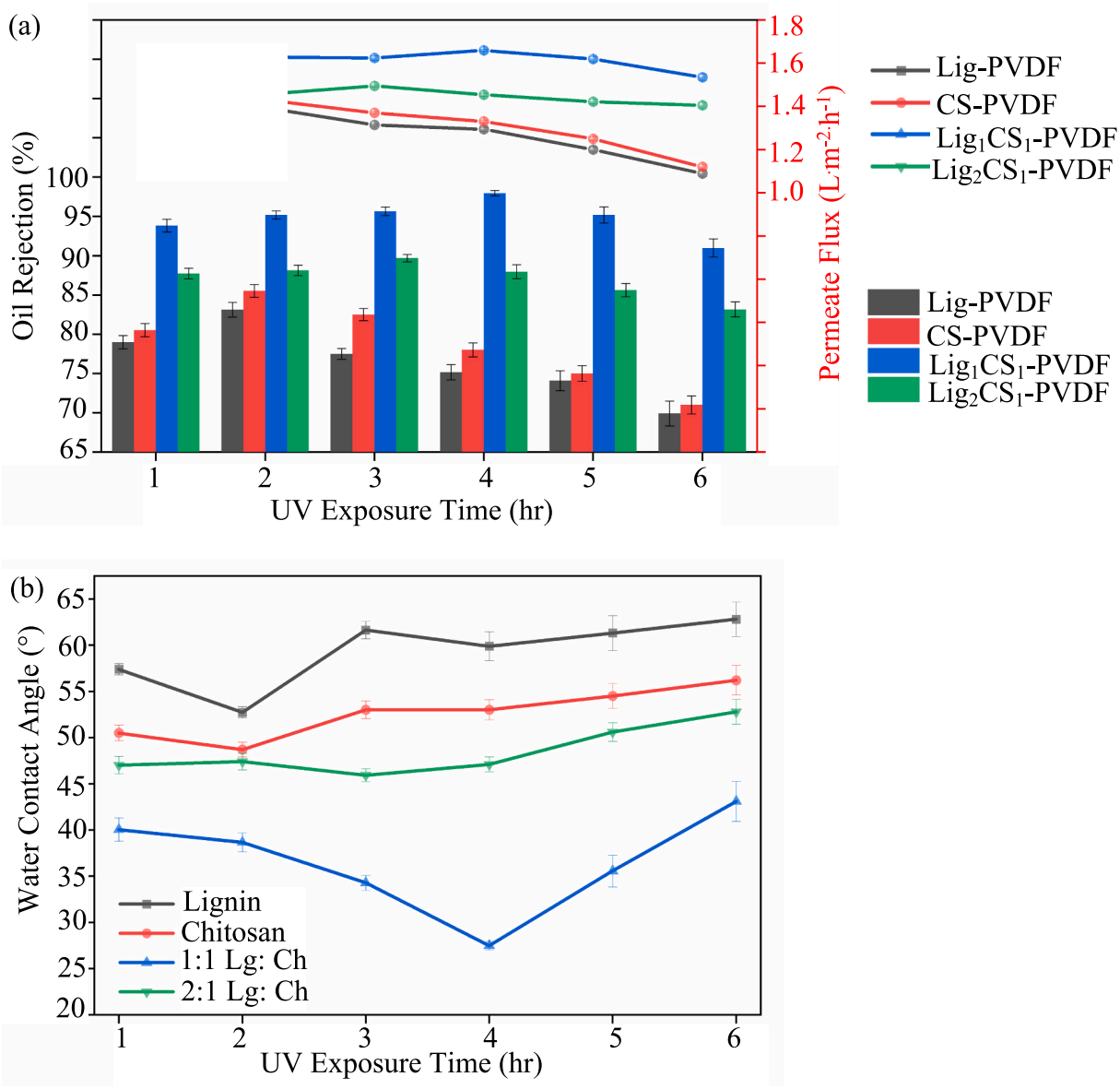

Fig. 6. Effects of UV exposure time on (a) oil rejection, permeate flux, and (b) water contact angle of lignin and/or chitosan-coated PVDF HFMs under PEC activation (0.2 g/L TiO_2, 0.5 vol% H_2O_2, and 3 V).

solution under UV irradiation and DC bias. The generated reactive oxygen species (ROS) further oxidized the surface and enhanced hydrophilicity [28,29]. This dual-modification approach was designed to improve membrane wettability, reduce fouling, and enhance oil–water separation performance.

The surface morphology and elemental composition of pristine and modified PVDF HFMs were evaluated using SEM and EDX, as shown in Fig. 2. The pristine PVDF HFMs (Fig. 2a–c) exhibited a smooth surface and a composition dominated by fluorine (55.3 wt%), with relatively low carbon (34.7 wt%) and oxygen (10.0 wt%), reflecting the intrinsic hydrophobicity of the fluoropolymer. Following surface coating with lignin (Fig. 2(d)–(f)), a slight decrease in fluorine (52.6 wt%) and an increase in carbon (37.3 wt%) and oxygen (10.1 wt%) contents were observed. This is attributed to the partial coverage by lignin, a polyphenolic compound rich in oxygenated functionalities. Chitosan-coated PVDF (Fig. 2(g)–(i)) exhibited a similar elemental profile (53.8 wt% F, 36.5 wt% C, 9.7 wt% O). Notably, the lignin–chitosan composite coatings led to more substantial changes. The Lig_1CS_1-PVDF HFMs (Fig. 2(j)–(l)) showed a pronounced reduction in fluorine (47.3 wt%) and an increase in carbon (40.3 wt%) and oxygen (12.4 wt%). The result suggests a synergistic effect between lignin and chitosan, resulting in a denser and more functionalized coating. In contrast, increasing the content to a 2:1 ratio (Lig_2CS_1) resulted in slightly higher fluorine content (49.1 wt%) and lower oxygen (11.3 wt%), due to potential lignin aggregation. These modifications were further influenced by PEC treatment. PEC treatment generates ROS from TiO_2/H_2O_2 under UV irradiation and applied bias. These ROS facilitated oxidative functionalization of the membrane surface, enriching oxygen-containing groups and enhancing hydrophilicity [30]. The observed increase in surface oxygen content across biopolymer-coated membranes aligns with this mechanism and is expected to improve membrane wettability, fouling resistance, and oil–water separation performance [31,32].

To complement the morphological observations and decouple the effects of biopolymer coating and PEC activation, XPS was performed on pristine PVDF, Lig1CS1-PVDF, and PEC-modified Lig1CS1-PVDF HFMs, as shown in Fig. 3. In the C 1s spectra [Fig. 3(a)–(c)(i)], pristine PVDF exhibited three main components assigned to C—C/C—H (~284.68 eV), CF_2 (~288.51 eV), and C-CF_2 (~290.9 eV), characteristic of the

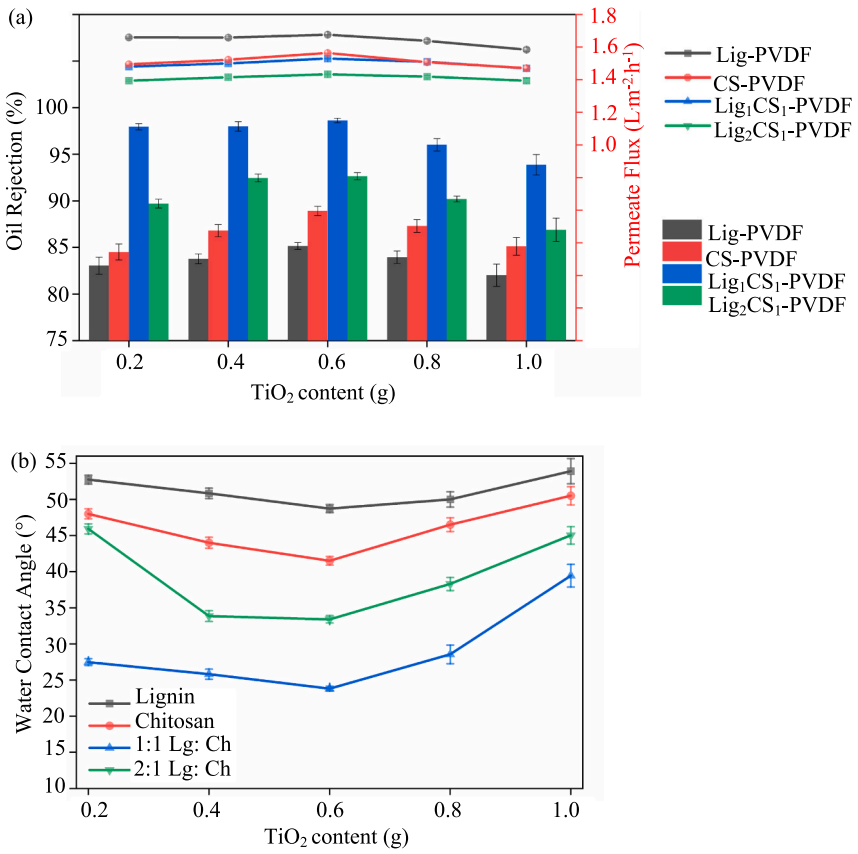

Fig. 7. Effects of TiO_2 content on (a) oil rejection, permeate flux, and (b) water contact angle of lignin and/or chitosan-coated PVDF HFMs under PEC activation (0.5 vol% H_2O_2, 3 V, and 4 h UV).

fluoropolymer backbone. After coating, the intensity of the CF_2 and C-CF_2 peaks decreased, while new C—O/C—N (~285.93 eV) components appeared, confirming the introduction of oxygen- and nitrogen-containing groups from lignin and chitosan. Following PEC activation, the CF_2 and C-CF_2 peaks further decline while the C—O/C—N component became more prominent. The decline indicates further oxidation of the surface and partial replacement of fluorinated carbon with polar functionalities. The O 1s spectra [Fig. 3(a)–(c)(ii)] of pristine PVDF showed two peaks at ~532.8 eV (C—O/–OH) and ~531.5 eV (C═O). Upon coating and PEC activation, the proportion of the C—O/C═O species increased due to the presence of phenolic, hydroxyl, and amide functionalities from the biopolymers and PEC treatment. The N 1s spectra [Fig. 3(a–c)iii] further verified these changes. No nitrogen signal was detected for pristine PVDF, whereas a distinct peak near 399.6–399.8 eV appeared for the biopolymer-coated and PEC-activated membranes. This distinct peak was induced by –NH/–NH_2 and amide (N—C═O) groups originating from chitosan. The XPS results clearly distinguish the chemical changes introduced by biopolymer coating and PEC activation, confirming the formation of oxygen-rich functionalities on the membrane surface. To further evaluate how these surface modifications influence the bulk stability and structural characteristics, additional characterization was carried out on the final PEC-modified PVDF HFMs.

The CLSM height maps (Fig. 4(a)–(e)) reveal the progressive surface modification of PVDF HFMs after lignin and chitosan coating. The color gradients represent height variations, where red–white zones correspond to raised regions and blue–green zones to valleys. The pristine PVDF (Fig. 3(a)) shows distinct peaks and depressions, indicating a rough and open surface. The Lig-PVDF (Fig. 3(b)) and CS-PVDF (Fig. 3(c)) membranes display smoother and more uniform topographies, although minor localized valleys remain. The co-blended membranes, Lig1CS1-PVDF (Fig. 3(d)) and Lig2CS1-PVDF (Fig. 3(e)), exhibit broader red–yellow plateaus and shallower valleys, implying increased surface texturing and coating continuity. Quantitatively, as shown in Fig. 3(f), the S_a increased from 1.67 μm (PVDF) to 2.67 μm (Lig1CS1-PVDF). Meanwhile, the S_{mr} shifted from 2.06 % for PVDF to 2.63 % for Lig1CS1-PVDF and further to 9.72 % for Lig2CS1-PVDF. The sharp increase in S_{mr} indicates a more compact and load-bearing surface for Lig2CS1-PVDF, likely due to over-densification of lignin. These morphological trends are consistent with the EDX results, verifying that lignin–chitosan co-deposition leads to a more compact surface layer.

Fig. 5(a) displays the thermal stability of pristine and modified PVDF HFMs. The pristine PVDF HFMs showed a single-step degradation beginning at approximately 450 °C, corresponding to the decomposition of the PVDF polymer backbone. The residual mass at 800 °C is approximately 20 %, indicative of the high thermal resistance and char-forming nature of the base polymer [33]. In contrast, the Lig-PVDF HFMs displayed a two-step degradation profile. An early mass loss that occurred between 100 and 150 °C could be attributed to the degradation of low molecular weight lignin fragments and volatile impurities [34]. The second major degradation event, observed around 450 °C, corresponds to PVDF decomposition. Notably, this sample exhibits the lowest final residue (~5 %). The outcome suggested that lignin, when used alone, may facilitate a more complete thermal decomposition. This behavior could be linked to the catalytic effects of lignin's phenolic structures, which may destabilize the PVDF matrix during pyrolysis [35]. The CS-PVDF HFMs also presented a two-stage degradation behavior (Fig. 5b). The initial weight loss near 150 °C is due to the evaporation of bound moisture and degradation of labile amine or acetyl groups in chitosan [36]. The second degradation stage occurs near 450 °C, similar to pristine PVDF, and is associated with main chain scission. The final residue is slightly higher than that of Lg-PVDF

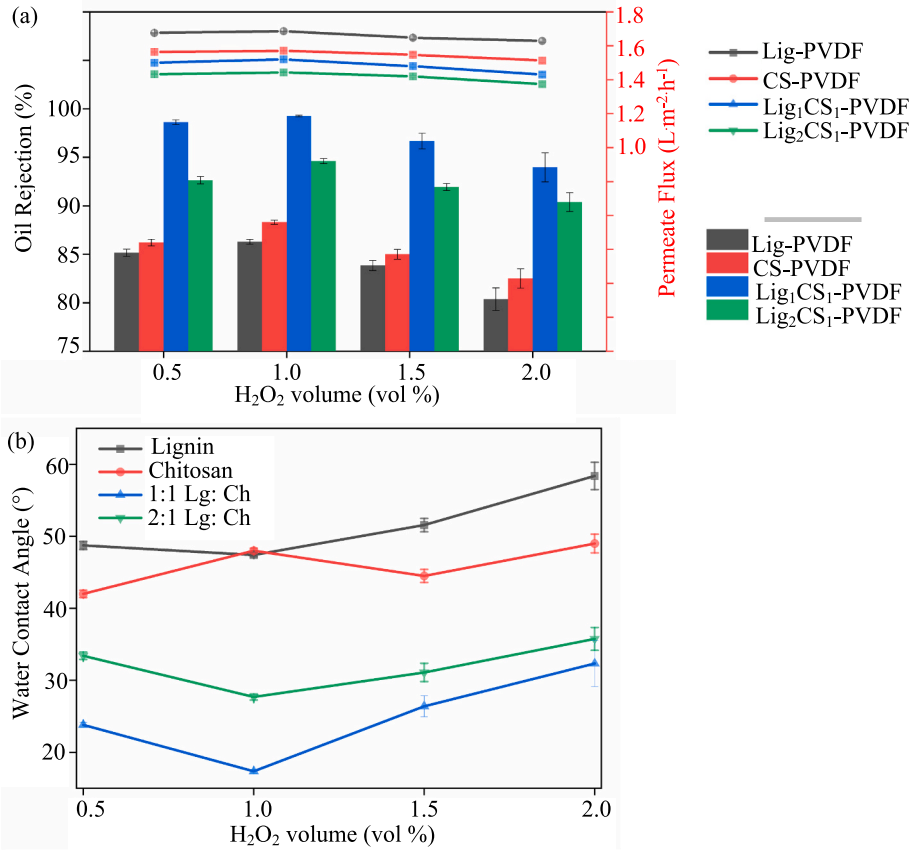

Fig. 8. Effects of H_2O_2 volume on (a) oil rejection, permeate flux, and (b) water contact angle of lignin and/or chitosan-coated PVDF HFMs under PEC activation (0.6 g/L TiO_2, 3 V, and 4 h UV).

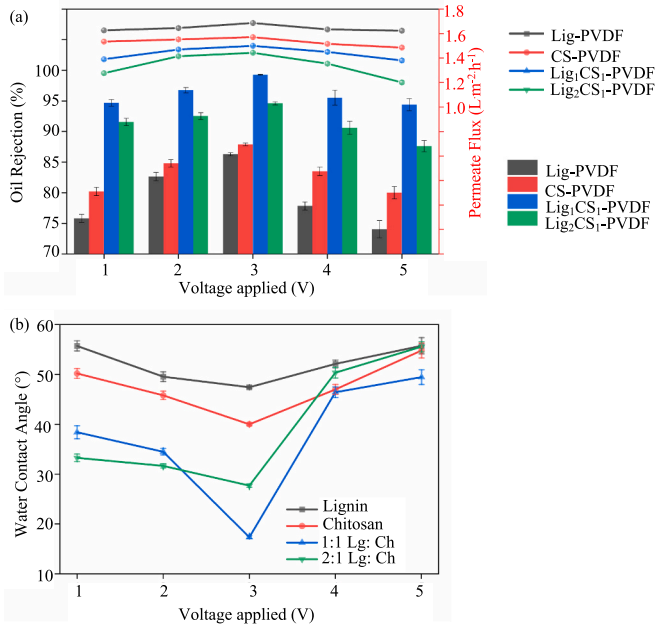

Fig. 9. Effects of voltage applied on (a) oil rejection, permeate flux, and (b) water contact angle of lignin and/or chitosan-coated PVDF HFMs under PEC activation (0.6 g/L TiO_2, 0.5 vol% H_2O_2, and 4 h UV).

HFMs, indicating that chitosan imparts moderate thermal stability, potentially through intermolecular hydrogen bonding or limited barrier effects [37]. The Lig_1CS_1-PVDF HFMs exhibited the most thermally stable profile among all modified membranes. The early-stage weight loss is minimal, and major degradation occurs in the 400–500 °C range. The residual mass at 800 °C is approximately 15 %, comparable to that of pristine PVDF. This improved performance is likely due to synergistic interactions between lignin and chitosan within the polymer matrix, enhancing thermal resistance through cross-linking or network formation that suppresses chain mobility and degradation.

XRD analysis was performed to investigate the crystalline phases and structural changes in the pristine and coated PVDF HFMs. As shown in Fig. 5(c), the diffraction pattern of pristine PVDF HFMs corresponding to the γ-phase PVDF, in accordance with ICCD No. 00-061-1406. The γ-phase crystalline structure is known for its mixed polar properties and intermediate conformation between the non-polar α-phase and the highly polar β-phase. The presence of γ-phase PVDF is particularly advantageous in membrane applications due to its balance of mechanical strength and surface polarity [38]. Incorporation of lignin and/or chitosan did not alter the γ-phase features, indicating that the bulk crystalline phase of PVDF remained intact. However, notable differences in peak intensity and broadening were observed. CS-PVDF HFMs and LigCS-PVDF HFMs showed reduced peak intensity and increased peak width, suggesting a reduction in crystallinity and enhanced amorphous content. This may be due to hydrogen bonding or electrostatic interactions between the PVDF chains and the functional groups in lignin (phenolic –OH) and chitosan (–NH_2 and –OH), which interfere with regular chain packing. The Lig_1CS_1-PVDF HFMs exhibited the most significant disruption of crystallinity, indicating stronger synergistic effects between lignin and chitosan in the polymer matrix. This reduction in crystallinity may enhance the hydrophilicity, interfacial adhesion, and permeability of the membranes [39].

FTIR spectra of PVDF HFMs with and without PEC modification are presented in Fig. 5(d). The pristine PVDF exhibited characteristic

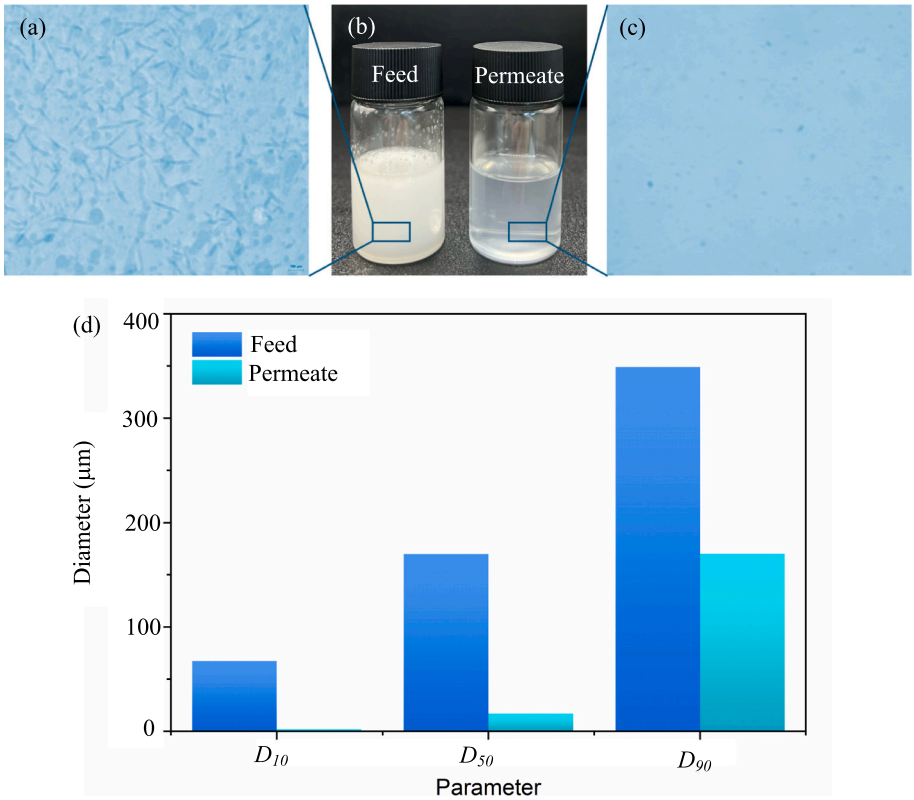

Fig. 10. (a) Optical microscope image of the feed emulsion, (b) photograph of the feed and permeate emulsions, (c) optical microscope image of the permeate emulsion, and (d) comparison of D_{10}, D_{50}, and D_{90} droplet diameters for feed and permeate. All samples were tested using PEC-modified Lig_1CS_1-PVDF HFMs (0.6 g·L^{-1} TiO_2, 1.0 vol% H_2O_2, 3 V, 4 h UV).

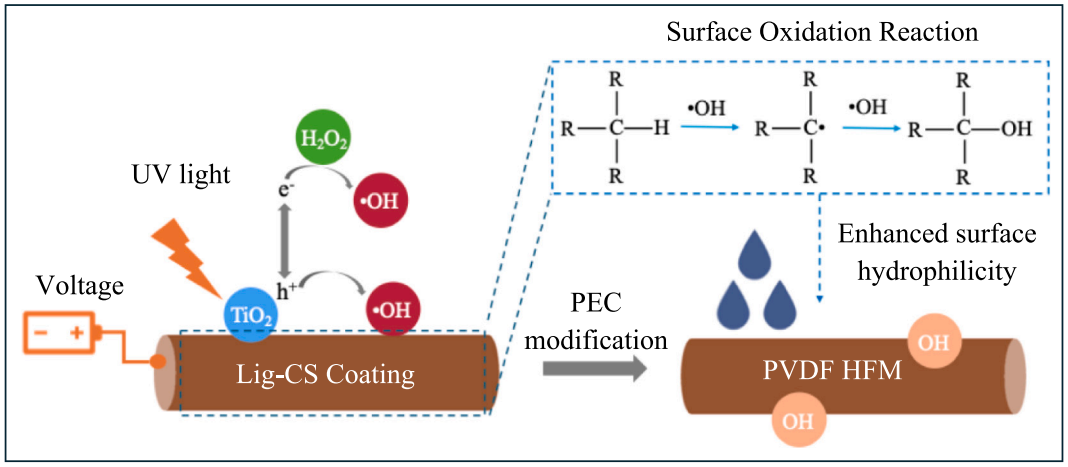

Fig. 11. The proposed mechanism during PEC activation of lignin and/or chitosan-coated PVDF HFMs.

absorption bands at ~2970–2850 cm^{-1} (C—H stretching), 1500 cm^{-1} and 880 cm^{-1} (CF_2 bending), consistent with the γ-phase structure. Upon lignin incorporation (Lig-PVDF), additional peaks emerged near 1600 cm^{-1}, corresponding to aromatic C=C stretching of lignin units. Besides, the O—H stretching band at 3400 cm^{-1} indicates the introduction of phenolic groups from lignin. Chitosan-coated PVDF (CS-PVDF) displayed a broad O—H/N—H stretching band at 3200–3500 cm^{-1} besides new peaks at ~1650 cm^{-1} and ~1580 cm^{-1}. The new peaks are assignable to amide I (C=O) and amide II (N—H) vibrations, respectively. With lignin-chitosan composite coating, the Lig_1CS_1-PVDF HFMs exhibited both aromatic and amide-related bands due to the coexistence of phenolic and amino functionalities, respectively. Among the modified membranes, the relative intensity of PVDF's CF_2 absorptions decreased. The decrement suggests strong hydrogen bonding and electrostatic interactions between PVDF chains and the introduced biopolymers. These spectral changes verify the successful immobilization of lignin and chitosan on the PVDF surface. The verification was further supported by the enhanced oxygen content observed by EDX and the reduced crystallinity seen in XRD.

3.2. *Influence of PEC parameters on oil–water separation performance*

The impact of UV exposure duration on membrane performance is illustrated in Fig. 6. All modified PVDF HFMs showed improved oil

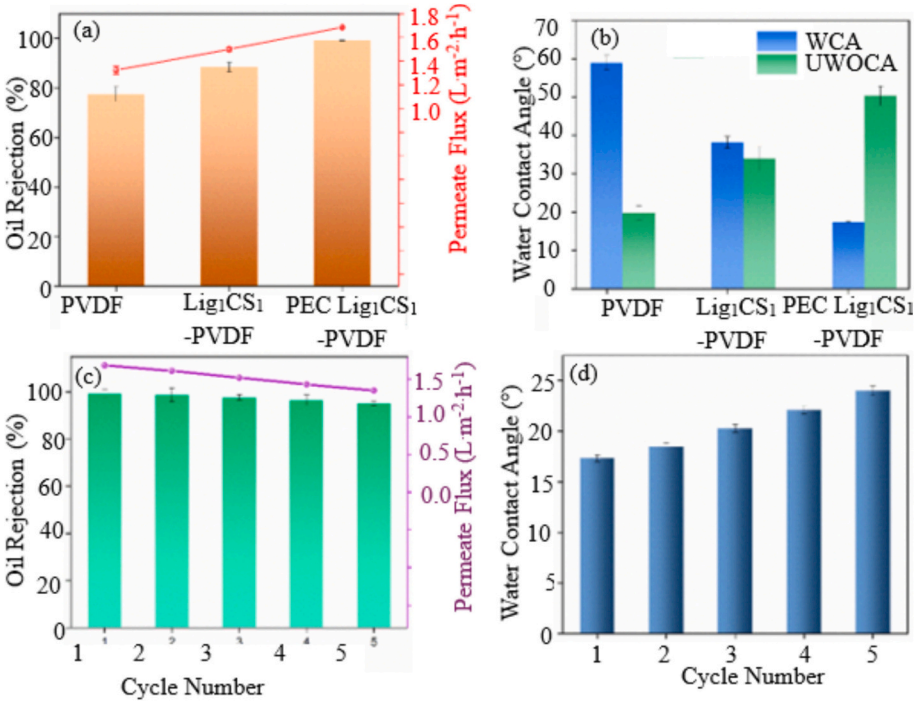

Fig. 12. (a) Performance and (b) wettability comparison of pristine PVDF, Lig_1CS_1-PVDF, and PEC-modified Lig_1CS_1-PVDF HFMs (0.6 g·L^{-1} TiO_2, 1.0 vol% H_2O_2, 3 V, 4 h UV). (c, d) Reusability performance of Lig_1CS_1-PVDF HFMs over five cycles.

rejection and permeate flux with increasing exposure time from 1 to 3 h, driven by enhanced photoactivation and formation of ROS (e.g., •OH) that increased surface hydrophilicity and reduced fouling. However, a further increase to 4 h led to a slight decline in performance for most formulations, likely due to overexposure, leading to biopolymer degradation and pore structure damage. Interestingly, the Lig_1CS_1-PVDF HFMs remained stable and showed their best overall performance at 4 h, maintaining high oil rejection (96.88 ± 0.63 %), flux (1.65 ± 0.02 $L{\cdot}m^{-2}{\cdot}h^{-1}$), and hydrophilicity (WCA = 28.6 ± 1.1°). This indicates that the synergistic effect of lignin and chitosan at a 1:1 ratio provides a robust coating capable of withstanding longer PEC activation while maximizing membrane performance.

The influence of TiO_2 dosage on the PEC performance of coated PVDF hollow fiber membranes is shown in Fig. 7. Among all formulations, Lig_1CS_1-PVDF HFMs exhibited the highest oil rejection (96.81 ± 0.83 %) and permeate flux (1.66 ± 0.01 $L{\cdot}m^{-2}{\cdot}h^{-1}$) at 0.6 g TiO_2, indicating an optimal activation point. Oil rejection and flux slightly declined beyond this dosage for all samples. Similarly, the lowest water contact angle (25.9 ± 0.7°) was also observed for Lig_1CS_1-PVDF at 0.6 g, reflecting improved surface wettability. A general trend of decreased WCA with increasing TiO_2 loading up to 0.6 g, followed by a gradual rise, was consistent across all formulations. This enhancement is commonly attributed to increased surface activation via hydroxyl radical formation during PEC treatment, as reported in previous studies [18,40]. Beyond the 0.6 g threshold, reduced performance may stem from increased light scattering and shielding by excess TiO_2 particles, which can inhibit effective UV penetration and ROS generation. Additionally, high TiO_2 concentrations may promote particle agglomeration, reducing active surface area for photocatalytic reactions [41].

H_2O_2 was employed as an oxidizing agent during PEC pre-activation to enhance the generation of ROS radicals via photolysis and TiO_2-catalyzed decomposition. As shown in Fig. 8, increasing the H_2O_2 volume from 0.5 to 1.0 vol% improved the membrane performance. The effect is obvious, particularly for the Lig_1CS_1-PVDF HFMs, which achieved peak oil rejection of 96.65 ± 0.87 % and flux of 1.64 ± 0.01 $L{\cdot}m^{-2}{\cdot}h^{-1}$. This is attributed to the synergistic interaction between H_2O_2 and UV-activated TiO_2, which accelerates the formation of ROS and enhances surface hydroxylation. Unlike post-treatment methods, this PEC step does not remove surface contaminants but rather serves to activate the surface of the biopolymer-coated membrane by generating reactive species that promote hydrophilic functionalization. However, higher H_2O_2 concentrations beyond 1.0 vol% led to reduced performance, possibly due to the quenching of hydroxyl radicals and biopolymer degradation [42,43]. WCA results supported this trend, with the lowest contact angle (19.2 ± 0.9°) observed at 1.0 vol% H_2O_2, indicating a highly hydrophilic surface ideal for oil–water separation.

The effect of applied voltage during PEC activation is depicted in Fig. 9. Increasing the voltage from 1 V to 3 V enhanced oil rejection and permeate flux across all membrane types, with the Lig_1CS_1-PVDF HFMs again outperforming others by achieving 96.52 ± 0.69 % oil rejection and 1.67 ± 0.02 $L{\cdot}m^{-2}{\cdot}h^{-1}$ flux at 3 V. The electric field likely promoted electron–hole separation in TiO_2, intensifying ROS formation and surface hydroxylation. However, further increase of voltage to 4–5 V led to diminished performance. The diminished performance could be attributed to excessive electrochemical stress and localized Joule heating at the electrode–solution interface, which accelerated charge recombination [44]. When the voltage was too high, the strong electric field pushes electrons and holes to move fast, making them more likely to collide and recombine before producing ROS. The heat generated at high voltage also increased the recombination by disturbing charge stability. In addition, the high voltage caused charge build-up on the TiO_2 surface, which led to the reverse flow of electrons and further loss of active charges [45]. The heat buildup under prolonged operation at the high voltage could also induce partial deterioration of TiO_2-based layers, reducing PEC stability and hydrophilicity [46]. The WCA trend showed a sharp decrease up to 3 V, reaching 20.1 ± 1.2°, followed by an increase at higher voltages, consistent with the reduction in surface hydrophilicity.

Across all parameters tested, the Lig_1CS_1-PVDF HFMs formulations consistently delivered the highest oil–water separation performance under PEC treatment. Optimal conditions were identified as UV exposure of 4 h, TiO_2 content of 0.6 g, H_2O_2 volume of 1.0 vol%, and applied voltage of 3 V. These conditions facilitated maximum radical formation and surface activation, resulting in significant improvements in oil

rejection, water permeability, and membrane hydrophilicity. Fine-tuning of PEC variables was able to improve the efficacy of PVDF HFMNs membranes in oil-water treatment. To further confirm the involvement of ROS during PEC activation, radical scavenger inhibition experiments were performed using Lig1CS1-PVDF HFMs after PEC activation (0.6 g/L TiO_2, 1.0 vol% H_2O_2, 3 V, 4 h). As shown in Fig. S1, the presence of scavengers suppressed both surface hydrophilization and separation performance compared to the scavenger-free control. The inhibition trend followed t-BuOH > BQ > EDTA, indicating that •OH was the dominant species responsible for surface oxidation.

The optical microscope images in Fig. 10(a) and (c) illustrate the morphological changes in the oil-in-water emulsion before and after separation. The feed emulsion (Fig. 10(a)) exhibited numerous large and coalesced oil droplets, whereas the permeate (Fig. 10(c)) showed only fine and sparsely distributed droplets with greatly reduced density and size. The visual comparison of the feed and permeate emulsions (Fig. 10(b)) also demonstrated a clear decrease in turbidity. To further quantify these observations, the particle size distribution of the emulsions was evaluated, as shown in Fig. 10(d). The feed exhibited a broad droplet size distribution (D_{10} = 67.3 μm, D_{50} = 169.9 μm, D_{90} = 348.9 μm, mean = 189.9 μm), whereas the permeate displayed a markedly narrow distribution with significantly smaller droplets (D_{10} = 2.17 μm, D_{50} = 17.14 μm, D_{90} = 170.15 μm, mean = 61.45 μm). About 90 % reduction in D_{50} confirms the high oil rejection efficiency of the Lig_1CS_1-PVDF membrane. The combined evidence from optical microscopy and particle size analysis is in agreement with the high oil rejection and improved hydrophilicity results discussed earlier.

The proposed mechanism of the PEC activation process is illustrated in Fig. 11. Under UV irradiation, TiO_2 nanoparticles in the reacting medium generate photoinduced electrons (e^-) and holes (h^+). The applied electrical bias facilitates charge separation by driving the electrons toward the cathode and holes toward the anode, thereby suppressing recombination and sustaining continuous redox reactions. The photogenerated holes react with surface-adsorbed water molecules (H_2O) to produce highly reactive •OH, while the electrons reduce H_2O_2 to form additional •OH species. These ROS oxidize the organic components of the lignin and/or chitosan coating, introducing hydroxyl (–OH) functional groups onto the membrane surface. The surface hydroxylation increases surface polarity and hydrophilicity, improving water permeability and reducing oil fouling during filtration.

3.3. Membrane stability assessment

Fig. 12 illustrates the comparative and cyclic performance among pristine PVDF HFMs, Lig_1CS_1-PVDF HFMs and PEC modified Lig_1CS_1-PVDF HFMs. Pristine PVDF HFMs exhibited a baseline oil rejection of ~78 %, which significantly improved to ~88 % following biopolymer modification (1:1 ratio of lignin: chitosan). Upon PEC activation, oil rejection further increased to ~97 %, affirming the synergistic effect of surface coating and radical-mediated activation in enhancing separation efficiency. A similar trend was observed for permeate flux, which improved progressively from ~1.3 $L{\cdot}m^{-2}{\cdot}h^{-1}$ (pristine PVDF HFMs) to ~1.4 $L{\cdot}m^{-2}{\cdot}h^{-1}$ (Lig_1CS_1-PVDF HFMs), and peaked at ~1.68 $L{\cdot}m^{-2}{\cdot}h^{-1}$ with PEC-treated Lig_1CH_1-PVDF HFMs. The result demonstrated the dual benefit of structural and chemical surface enhancement. The wettability of the PVDF, Lig_1CS_1-PVDF, and PEC-activated Lig_1CS_1-PVDF HFMs was evaluated by measuring the WCA in air and the UWOCA in water, as shown in Fig. 10(b), with corresponding photographs shown in Fig. S2. The pristine PVDF membrane exhibited a WCA of 63.18°. After modification with lignin and chitosan (Lig_1CS_1-PVDF), the WCA decreased to 36.39°, indicating the successful introduction of hydrophilic functional groups. Subsequent PEC activation further reduced the WCA to 17.19°, confirming a highly hydrophilic surface due to the generation of additional oxygen-containing species. In contrast, the UWOCA increased from 19.75° (PVDF) to 33.96° (Lig_1CS_1-PVDF) and 50.36° (PEC Lig_1CS_1-PVDF), revealing enhanced underwater oleophobicity after modification and activation. This dual change indicates that the surface became more hydrophilic and less oil-adhesive, facilitating selective water permeation while effectively repelling oil droplet.

Importantly, the reusability performance across five treatment cycles for PEC-treated Lig_1CS_1-PVDF HFMs (Fig. 9(c) and (d)) revealed remarkable stability. Oil rejection remained consistently above 93 %, and flux experienced only a minor reduction (<7 %) over five cycles. The contact angle gradually increased from 20° to 25° (Fig. 9d), likely due to minor surface fouling or coating degradation. However, the change remained within acceptable operational limits. These findings affirm the durability and practical potential of PEC-activated Lig_1CH_1-PVDF HFMs for repeated oil–water separation.

The chemical, thermal, and matrix stability of the Lig1CS1-PVDF HFMs were assessed to verify their durability under practical conditions (Fig. S3). In the presence of HCl, NaOH, or ethanol (Fig. S3(a) and (b)), the membranes still exhibited strong stability, maintaining oil rejection above 90 %. Exposure to 1 M HCl and ethanol caused negligible changes. A moderate decline of about 8 % in rejection and a slight increase in WCA were observed in NaOH, attributed to partial lignin dissolution [47] and chitosan deprotonation [48]. Thermal stability tests (Fig. S3(c) and (d)) showed minor performance variations with temperature. Oil rejection decreased slightly from 99.26 % to 97.9 % as the permeate flux increased with temperature. The increase in permeate flux at a higher temperature is due to the reduced viscosity. Water could flow through slightly expanded pores easily. However, the small drop in oil rejection occurred because oil droplets could more easily penetrate the membrane under these conditions [49]. Meanwhile, WCA rose marginally. The heat can loosen the bonds between chitosan and lignin on the membrane surface, making it less hydrophilic. In the presence of NaCl and/or surfactant (Fig. S3(e) and (f)), oil rejection decreased progressively, reaching 91.45 % in 5 % NaCl, 88.45 % in 0.1 % SDS, and 80.35 % in the combined saline and surfactant feed, corresponding to an 8–20 % reduction relative to the control. The decrease in oil rejection under salinity and wetting changes was mainly caused by the reduced charge screening and the surface adsorption effects [50]. With the increasing salinity, ions compress the electrical double layer and reduce electrostatic repulsion between oil droplets and the membrane. Surfactant molecules adsorbed onto the membrane surface mask hydrophilic sites with a thin hydrophobic layer. Despite this, the membranes still maintained more than 80 % rejection and WCA values below 22°, indicating slight antifouling and interfacial stability.

4. Conclusions

This study presents the successful fabrication and optimization of PEC-activated PVDF HFMs coated with a lignin and chitosan biopolymer blend for efficient oil–water separation. Morphological, thermal, and crystalline characterization confirmed the structural integrity and synergistic enhancement of membrane properties via dual biopolymer coating and PEC treatment. The Lig_1CH_1-PVDF HFMs composition offered the most uniform surface morphology, minimized surface roughness, and induced favourable microstructural features that improved hydrophilicity and reduced fouling tendencies. TGA results revealed enhanced thermal stability of LigCS-PVDF HFMs, while XRD analysis indicated decreased crystallinity and increased amorphous content. These changes in membrane properties contributed to the improved water permeability and interfacial interactions. PEC treatment under optimized conditions (0.6 g/L TiO_2, 1.0 vol% H_2O_2, 3 V, 4 h UV) activated the membrane surface via ROS generation, enhancing surface polarity and eliminating organic contaminants. The resulting membranes demonstrated remarkable performance of 99.26 % oil rejection, 1.69 $L{\cdot}m^{-2}{\cdot}h^{-1}$ permeate flux, a low contact angle of 17.34°, and strong reusability over five cycles. These findings underscore the critical role of material synergy and PEC surface engineering in advancing membrane-based oily wastewater treatment. This work

highlights a promising strategy toward the development of high-efficiency, low-fouling membranes tailored through rational biopolymer design and ROS-mediated surface activation.

Supplementary data to this article can be found online at https://doi.org/10.1016/j.jwpe.2025.109293.

CRediT authorship contribution statement

Sin Ling Chiam: Writing – original draft, Methodology, Investigation, Data curation. **Pei Yee Wong:** Investigation, Data curation. **Yan Xu:** Supervision, Methodology, Conceptualization. **C.P. Leo:** Writing – review & editing, Validation, Supervision, Conceptualization. **Swee-Yong Pung:** Writing – review & editing, Data curation.

Declaration of competing interest

The authors declare that they have no known competing financial interests or personal relationships that could have appeared to influence the work reported in this paper.

Acknowledgments

This work is the output of the http://www.nict.go.jp/en/asean_ivo/index.html project, ICT-Driven Water Quality Monitoring Systems: Enhancing Precision and Sustainability under the Climate Change, financially supported by NICT (http://www.nict.go.jp/en/index.html). The authors would like to further thank Universiti Sains Malaysia for providing a postdoctoral fellowship to Dr. Chiam Sin Ling.

Data availability

Data will be made available on request.

References

[1] M. Chen, S.G. Heijman, L.C. Rietveld, Ceramic membrane filtration for oily wastewater treatment: basics, membrane fouling and fouling control, Desalination 583 (2024) 117727, https://doi.org/10.1016/j.desal.2024.117727.
[2] K. Abuhasel, M. Kchaou, M. Alquraish, Y. Munusamy, Y.T. Jeng, Oily wastewater treatment: overview of conventional and modern methods, challenges, and future opportunities, Water 13 (2021) 980, https://doi.org/10.3390/w13070980.
[3] S. Lustenberger, R. Castro-Muñoz, Advanced biomaterials and alternatives tailored as membranes for water treatment and the latest innovative European water remediation projects: a review, Case Stud. Chem. Environ. Eng. 5 (2022) 100205, https://doi.org/10.1016/j.cscee.2022.100205.
[4] Y. Wang, Y. Zhang, L. Liang, F. Tu, Z. Li, X. Tang, L. Dai, L. Li, Research progress on membrane separation technology for oily wastewater treatment, Toxics 12 (2024) 794, https://doi.org/10.3390/toxics12110794.
[5] L. Yan, X. Yang, H. Zeng, Y. Zhao, Y. Li, X. He, J. Ma, L. Shao, Nanocomposite hydrogel engineered hierarchical membranes for efficient oil/water separation and heavy metal removal, J. Membr. Sci. 668 (2023) 121243, https://doi.org/10.1016/j.memsci.2022.121243.
[6] B. Li, B. Qi, Z. Guo, D. Wang, T. Jiao, Recent developments in the application of membrane separation technology and its challenges in oil–water separation: a review, Chemosphere 327 (2023) 138528, https://doi.org/10.1016/j.chemosphere.2023.138528.
[7] R.A. Roslan, W.J. Lau, N.S. Mohd Nawi, E.N. Nxumalo, A.F. Ismail, Enhancing properties of PSF membrane via a simple two-step coating of PDA and PVP for separating oil/water emulsions, J. Chem. Technol. Biotechnol. 100 (2025) 37–49, https://doi.org/10.1002/jctb.7752.
[8] H. Rajabnia, A. Aroujalian, P. Salimi, Antifouling performance enhancement of PES membranes using hydrophilic nanoparticles of poly(dopamine-acrylate) for oil/water separation, J. Environ. Chem. Eng. 12 (2024) 112797, https://doi.org/10.1016/j.jece.2024.112797.
[9] Y. Zhang, J. Cui, H. Sun, A. Xie, C. Li, C. Xue, J. Pan, Superwetting polypropylene fiber membrane modified with Co-doped β-FeOOH nanorods for enhanced oil/water separation and self-cleaning, Mater. Today Chem. 38 (2024) 102050, https://doi.org/10.1016/j.mtchem.2024.102050.
[10] S. Shen, Q. Fan, H. Li, L. Xu, G. Zhang, R. Bai, Simple surface modification of PVDF membrane via a quaternization of NM88B for efficient oil/water separation, J. Water Process Eng. 61 (2024) 105352, https://doi.org/10.1016/j.jwpe.2024.105352.
[11] I.A. Khan, W. Falath, N. Baig, I. Aljundi, Modification of PVDF membranes using polyvinyl alcohol-crosslinked functionalized nano-silica sheets: high flux and antifouling properties for efficient oil–water separation, J. Taiwan Inst. Chem. Eng. 163 (2024) 105636, https://doi.org/10.1016/j.jtice.2024.105636.
[12] A. Das, S. Ghosh, N. Pramanik, Chitosan biopolymer and its composites: processing, properties and applications — a comprehensive review, Hybrid Adv. 6 (2024) 100265, https://doi.org/10.1016/j.hybadv.2024.100265.
[13] X. Liu, Z. Zou, D. Wang, D. Du, Z. Li, W. Li, Sustainable fabrication of chitosan membranes with optimized performance for ultrafiltration, Sep. Purif. Technol. 330 (2024) 125276, https://doi.org/10.1016/j.seppur.2023.125276.
[14] R. Hardian, A. Alammar, T. Holtzl, G. Szekely, Fabrication of sustainable organic solvent nanofiltration membranes using cellulose–chitosan biopolymer blends, J. Membr. Sci. 658 (2022) 120743, https://doi.org/10.1016/j.memsci.2022.120743.
[15] L. Cheng, X. Xu, Y. Jiang, S. Zhang, K. Xu, H. Wang, X. Zhang, R. Zhang, Z. Jiang, Antifouling membranes modified via chitosan derivatives for efficient oil-water separation, J. Membr. Sci. 727 (2025) 124082, https://doi.org/10.1016/j.memsci.2025.124082.
[16] J. Zhao, H. Liu, Y. Qi, R. Wang, Z. Lv, Y. Yu, S. Sun, Construction of robust DA@CNTs/CS hydrogel coatings on hydrophobic PVDF membrane by deposition of self-assembly for efficient separation of oil-water emulsion and dye wastewater, Sep. Purif. Technol. 333 (2024) 125956, https://doi.org/10.1016/j.seppur.2023.125956.
[17] J. Zeng, C. Wu, S. Wang, P. Li, J. Li, B. Wang, J. Xu, W. Gao, K. Chen, Development of high-throughput electrospun chitosan/PEO-CNC composite membranes with enhanced antibacterial and oil-water separation properties, Int. J. Biol. Macromol. 303 (2025) 140308, https://doi.org/10.1016/j.ijbiomac.2025.140308.
[18] Y. Xu, C. Leo, Z. Hu, C.-H. Hong, Photocatalytic valorization and cleaning of lignin coating on PVDF hollow fiber membranes for oil–water separation, Sep. Purif. Technol. 360 (2025) 131062, https://doi.org/10.1016/j.seppur.2024.131062.
[19] C. Qin, Y. Du, L. Xiao, Effect of hydrogen peroxide treatment on the molecular weight and structure of chitosan, Polym. Degrad. Stab. 76 (2002) 211–218, https://doi.org/10.1016/S0141-3910(02)00016-2.
[20] S.-M. Wang, Q.-Z. Huang, Q.-S. Wang, Study on the synergetic degradation of chitosan with ultraviolet light and hydrogen peroxide, Carbohydr. Res. 340 (2005) 1143–1147, https://doi.org/10.1016/j.carres.2005.02.009.
[21] Z. Ma, Y. Wu, Y. He, T. Wu, A novel protocol for the oxidative degradation of chitosan with hydrogen peroxide catalyzed by peroxomolybdate in aqueous solution, RSC Adv. 3 (2013) 12049–12051, https://doi.org/10.1039/C3RA40424B.
[22] G. Wang, S. Chen, H. Yu, X. Quan, Integration of membrane filtration and photoelectrocatalysis using a TiO_2/carbon/Al_2O_3 membrane for enhanced water treatment, J. Hazard. Mater. 299 (2015) 27–34, https://doi.org/10.1016/j.jhazmat.2015.06.005.
[23] F. De Brito, G.G. Bessegato, T.S. Viana, D.P. de Oliveira, C.A. Martínez-Huitle, M.V. B. Zanoni, Combination of photoelectrocatalysis and ozonation as a good strategy for organics oxidation and decreased toxicity in oil-produced water, J. Electrochem. Soc. 166 (2019) H3231–H3238, https://doi.org/10.1149/2.0331905jes.
[24] H. Xue, C. Ma, J. Liu, H. Yu, X. Yang, X. Zhang, S. Zhang, A promising device based on step stage theory for highly effective treatment of oil field wastewater, Chem. Technol. Fuels Oils 60 (2024) 610–618, https://doi.org/10.1007/s10553-024-01719-5.
[25] I.M. Idriss, Z. Hashmi, M.S.A. Bakar, N. Shamsuddin, A.L. Khan, F. Gapsari, T. D. Widodo, M.R. Bilad, Application of bio-based additives in membrane modification for water purification: a review, Next Mater. 8 (2025) 100836, https://doi.org/10.1016/j.nxmate.2025.100836.
[26] N. Zakaria, M.H. Hussin, A. Ahmad, C. Leo, P.E. Poh, K. Behzadian, I.I. Akinwumi, A. Moghayedi, J. Diazsolano, Lignin modified PVDF membrane with antifouling properties for oil filtration, J. Water Process Eng. 43 (2021) 102248, https://doi.org/10.1016/j.jwpe.2021.102248.
[27] C.E. Elhassani, A. El Gharrak, Y. Essamlali, S. Elamiri, K. Dânoun, S. Aboulhrouz, M. Zahouily, Lignin nanoparticles filled chitosan/polyvinyl alcohol polymer blend as a coating material of urea with a slow-release property, J. Appl. Polym. Sci. 140 (2023) e53755, https://doi.org/10.1002/app.53755.
[28] D.-T. Tran, J. Mendret, J.-P. Méricq, C. Faur, S. Brosillon, Study of permeate flux behavior during photo-filtration using photocatalytic composite membranes, Chem. Eng. Process. Process Intensif. 148 (2020) 107781, https://doi.org/10.1016/j.cep.2019.107781.
[29] R. Guo, W. Qin, B. Wang, L. Li, Q. Chen, Y. Tan, Y. Zhong, Z. Zhao, N. Liu, Z. Mo, NH_2-MIL-88B(Fe)/TiO_2/PAN electrostatically spun nanofiber membrane for photocatalytic degradation of tetracycline and oil–water separation, Sep. Purif. Technol. 351 (2024) 128059, https://doi.org/10.1016/j.seppur.2024.128059.
[30] L. Yang, D. Xu, X. Luo, X. Zhu, J. Zhao, J. Song, Y. Han, G. Li, X. Gao, L. Liu, Fe(II)-modulated microporous electrocatalytic membranes for organic microcontaminant oxidation and fouling control: mechanisms of regulating electron transport toward enhanced reactive oxygen species activation, Environ. Sci. Technol. 57 (2023) 19000–19011, https://doi.org/10.1021/acs.est.3c01792.
[31] X. Chen, H. Jia, Y. Zhan, F. Zhu, X. Duan, J. Liu, L. Li, Y. Li, Polyphenol assisted assembly of prussian blue analogs nanocrystals decorated 3D GO functional microspheres for polymer fiber bifunctional membrane with high oil–water emulsion permeability and powerful photocatalytic self-cleaning ability, J. Water Process Eng. 66 (2024) 105983, https://doi.org/10.1016/j.jwpe.2024.105983.
[32] Z. Al Ansari, L.F. Vega, L. Zou, Emulsified oil fouling resistant cellulose acetate–MoS_2-nanocomposite membrane for oily wastewater remediation, Desalination 575 (2024) 117335, https://doi.org/10.1016/j.desal.2024.117335.
[33] A.J. de Jesus Silva, M.M. Contreras, C.R. Nascimento, M.F. da Costa, Kinetics of thermal degradation and lifetime study of poly(vinylidene fluoride) (PVDF)

subjected to bioethanol fuel accelerated aging, Heliyon 6 (2020) e03771, https://doi.org/10.1016/j.heliyon.2020.e04573.
[34] J. López-Beceiro, A.M. Díaz-Díaz, A. Álvarez-García, J. Tarrío-Saavedra, S. Naya, R. Artiaga, The complexity of lignin thermal degradation in the isothermal context, Processes 9 (2021) 1154, https://doi.org/10.3390/pr9071154.
[35] L. Hu, T. Li, Y. Jing, Thermal pyrolysis behavior and decomposition mechanism of lignin revealed by stochastic cluster dynamics simulations, J. Phys. Chem. C 128 (2024) 3832–3838, https://doi.org/10.1021/acs.jpcc.3c07218.
[36] N.R. Araujo, R.C. Sebastiao, M.B. Freitas-Marques, W. da Nova Mussel, M. I. Yoshida, L.S. Virtuoso, Multilayer perceptron neural network applied to TG dynamic data of biopolymer chitosan — a robust tool to study the kinetics of solid thermal decomposition, Therm. Sci. Eng. Prog. 36 (2022) 101490, https://doi.org/10.1016/j.tsep.2022.101490.
[37] H. Ali, M.R. Dilshad, B. Haider, A. Islam, M.S. Akram, A. Jalal, S.N. Hussain, Preparation and characterization of novel polyamide-6/chitosan blend dense membranes for desalination of brackish water, Polym. Bull. 79 (2022) 4153–4169, https://doi.org/10.1007/s00289-021-03691-0.
[38] I. Sriyanti, R.F. Ramadhani, M.R. Almafie, M.K.N. Ap Idjan, E. Syafri, I. Solihah, M. R. Sanjaya, J. Jauhari, A. Fudholi, Physicochemical and mechanical properties of polyvinylidene fluoride nanofiber membranes, Case Stud. Chem. Environ. Eng. 9 (2024) 100588, https://doi.org/10.1016/j.cscee.2023.100588.
[39] D. Yue, H. Zhang, M. Liu, B. Li, Y. Ge, D. Sun, F. Li, A novel 5-sulfosalicylic acid–polyvinyl alcohol–hydroxyethyl cellulose vapor permeation membrane for gas dehumidification, Polymer 254 (2022) 125048, https://doi.org/10.1016/j.polymer.2022.125048.
[40] X. Zhang, C. Wei, S. Ma, C. Zhang, Y. Li, D. Chen, Z. Xu, X. Huang, Janus poly (vinylidene fluoride)-graft-(TiO_2 nanoparticles and PFDS) membranes with loose architecture and asymmetric wettability for efficient switchable separation of surfactant-stabilized oil/water emulsions, J. Membr. Sci. 640 (2021) 119837, https://doi.org/10.1016/j.memsci.2021.119837.
[41] R.V. Mikhaylov, P.E. Lavrik, V.N. Kuznetsov, N.I. Glazkova, Spectral dependence of UV light penetration into powder TiO_2 anatase, J. Photochem. Photobiol. A Chem. 430 (2022) 113954, https://doi.org/10.1016/j.jphotochem.2022.113954.
[42] G. Cheng, J. Wan, Q. Li, L. Sun, Y. Zhang, Z. Li, C. Dang, J. Fu, Degradation of reactive brilliant red X-3B by photo-Fenton-like process: effects of water chemistry factors and degradation mechanism, Water 14 (2022) 380, https://doi.org/10.3390/w14030380.
[43] H. Long, C. Larson, F. Coms, B. Pivovar, G. Dahlke, M. Yandrasits, Role of $H_3O^{\bullet}$ radical in the degradation of fuel cell proton-exchange membranes, ACS Phys. Chem. Au 2 (2022) 527–534, https://doi.org/10.1021/acsphyschemau.2c00037.
[44] B. Fu, J. Li, H. Jiang, X. He, Y. Ma, J. Wang, C. Hu, Modulation of electric dipoles inside electrospun $BaTiO_3$@TiO_2 core–shell nanofibers for enhanced piezo-photocatalytic degradation of organic pollutants, Nano Energy 93 (2022) 106841, https://doi.org/10.1016/j.nanoen.2021.106841.
[45] X. Zhou, Y. Zheng, J. Zhou, S. Zhou, Degradation kinetics of photoelectrocatalysis on landfill leachate using codoped TiO_2/Ti photoelectrodes, J. Nanomater. 2015 (2015) 810579, https://doi.org/10.1155/2015/810579.
[46] R. Habibi, N. Gilani, J.V. Pasikhani, A.E. Pirbazari, Improved photoelectrocatalytic activity of anodic TiO_2 nanotubes by boron in situ doping coupled with geometrical optimization: application of a potent photoanode in the purification of dye wastewater, J. Solid State Electrochem. 25 (2021) 545–560, https://doi.org/10.1007/s10008-020-04825-6.
[47] M. Qian, H. Lei, E. Villota, W. Mateo, Y. Zhao, E. Huo, Q. Zhang, X. Lin, Z. Huang, Optimization of delignification from Douglas fir sawdust by alkaline pretreatment with sodium hydroxide and its effect on structural and chemical properties of lignin and pyrolysis products, Bioresour. Technol. Rep. 8 (2019) 100339, https://doi.org/10.1016/j.biteb.2019.100339.
[48] E.A. Takara, J. Marchese, N.A. Ochoa, NaOH treatment of chitosan films: impact on macromolecular structure and film properties, Carbohydr. Polym. 132 (2015) 25–30, https://doi.org/10.1016/j.carbpol.2015.05.077.
[49] C.S. Ong, W.J. Lau, P.S. Goh, B.C. Ng, T. Matsuura, A.F. Ismail, Effect of PVP molecular weights on the properties of PVDF–TiO_2 composite membrane for oily wastewater treatment process, Sep. Sci. Technol. 49 (2014) 2303–2314, https://doi.org/10.1080/01496395.2014.928323.
[50] J.M. Dickhout, E. Virga, R.G. Lammertink, W.M. de Vos, Surfactant specific ionic strength effects on membrane fouling during produced water treatment, J. Colloid Interface Sci. 556 (2019) 12–23, https://doi.org/10.1016/j.jcis.2019.07.068.